Mistuned Response Prediction of Dual Flow-Path Integrally Bladed Rotors with Geometric Mistuning

Joseph A. Beck*
Manufacturing & Industrial Technologies Division
Air Force Research Laboratory
Wright-Patterson Air Force Base, Ohio 45433
Email: Joseph.Beck.8@us.af.mil

Jeffrey M. Brown
Senior Aerospace Engineer
Aerospace Systems Directorate
Turbine Engine Division
Air Force Research Laboratory
Wright-Patterson AFB, Ohio 45433
Email: Jeffrey.Brown.70@us.af.mil

Alexander A. Kaszynski
Aerospace Engineer
Aerospace Systems Directorate
Turbine Engine Division
Air Force Research Laboratory
Wright-Patterson AFB, Ohio 45433
Email: Alex.Kaszynski.ctr@us.af.mil

Joseph C. Slater
Professor and Interim Associate Vice President
for Career and Workforce Development
Dept. of Mechanical and Materials Engineering
Wright State University, Ohio 45435
Email: Joseph.Slater@wright.edu

Charles J. Cross
Chief, Turbine Engine Division
Aerospace Systems Directorate
Turbine Engine Division
Air Force Research Laboratory
Wright-Patterson AFB, Ohio 45433
Email: Charles.Cross.1@wpafb.af.mil

ABSTRACT

The geometric mistuning problem is investigated for dual flow-path integrally bladed rotors (DFIBRs) by outlining two methods that explicitly account for blade geometry surface deviations. The methods result in reduced-order models (ROMs) that are a reduced form of a parent Craig-Bampton component mode synthesis (CB-CMS) model. This is accomplished by performing a secondary modal analysis on different degrees of freedom (DOF) of the parent model. The DFIBR is formulated in cyclic symmetry coordinates with a tuned disk and ring and blades with small geometric deviations. The first method performs an eigen-analysis on the constraint DOF that provides a truncated set of interface modes, while the second method includes the disk and ring fixed interface normal mode in the eigen-analysis to yield a truncated set of ancillary modes. Utilization of tuned modes have the benefit of being

*Address all correspondence to this author.

solved in cyclic symmetry coordinates and only need to be calculated once, which offers significant computational savings for subsequent mistuning studies. Each geometric mistuning method relies upon the use of geometrically mistuned blade modes in the component mode framework to provide an accurate ROM. Forced response results are compared to both the full finite element model (FEM) solutions and a traditional frequency-based approach outlined in a previous effort. It is shown that the models provide highly accurate results with a significant reduction in solution time compared to the full FEM and parent ROM.

Nomenclature

Main Variables

N	=	Number of cyclic sectors
${}^{\bullet}N$	=	Number or size, where $\bullet$ is a placeholder for any variable
$\mathcal{M}$, $\mathcal{K}$, $\mathcal{F}$	=	Mass and stiffness matrix and external force vector, respectively, in CB-CMS modal coords.
E	=	Real-valued Fourier matrix
h	=	Harmonic index
$\mathbf{x}$, $\mathbf{p}$, $\mathbf{q}$	=	Physical, CB-CMS modal, and Secondary modal space DOF vectors, respectively

Overscripts

$\tilde{}$	=	Cyclic coordinates

Left Superscripts

D	=	Disk component
R	=	Ring component
I	=	Inner-blade component
O	=	Outer-blade component
A	=	All inner- and outer-blade components
CB	=	CB-CMS ROM matrices

Right Superscripts

a	=	blade index

Right Subscripts

n	=	CB-CMS fixed-interface normal mode DOF
c	=	CB-CMS constraint mode DOF
$\beta, \alpha, \tau, \sigma, \Gamma$	=	DOF index notation

1 Introduction

NEW turbine engine designs require innovative, variable cycles to push performance limits. This introduces multiple flow-paths that may require additional manipulation and energy. This is achieved with rotating engine components to further exchange mechanical energy with bypassed flow streams. This requires special rotating components, termed Dual Flow-path Integrally Bladed Rotors (DFIBRs), shown in Fig. 1, that are analogous to tradition Integrally Bladed Rotors

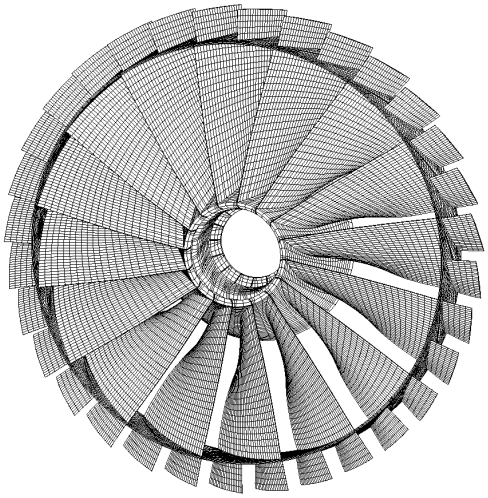

Fig. 1. Dual Flow-Path Integrally Bladed Rotor consists of an inner IBR and an integral outer ring with a second set of blades.

(IBRs). At the center of the DFIBR is a traditional IBR that has an integral ring attached to the tips of the inner-blades. A second set of integral blades are then attached to this outer-ring. As flow is bypassed around the inner-blades, the outer-blades can further energize the bypassed flow. These new integral components can have varying inner-to-outer blade count ratios and sizes. In addition, the inner- and outer-blades can be subject to different engine order excitations since they operate in different flow-fields and can be affected by different up- and down-stream flow disturbances. Beck, et al. [1] has shown these components have dynamic properties that are different from traditional IBRs, but they are just as susceptible to mistuning due the components' integral nature and subsequent lack of both material and friction damping.

A large body of research been devoted to mistuned response prediction of traditional IBRs with mistuning models derived from parent FEMs [2–9]. These methods introduced mistuning through perturbations to blade natural frequencies with elastic modulus perturbations resulting in a proportional change in a blade's natural frequencies, or through non-uniform, or non-proportional, frequency mistuning. These methods assume that an IBR's mistuned response can be approximated as a linear combination of tuned modes and are shown to work well in low excitation frequency ranges, provided blade geometric perturbations are small [10]. Beck, et al. [1] further expanded the frequency mistuning methods to DFIBRs using a CB-CMS approach to investigate the dynamic characteristics of DFIBRs. For traditional IBRs, these frequency mistuning methods can introduce errors when predicting fleet reliability [11]. To account for geometric perturbations, efforts have sought to better understand and predict mistuned response without the assumption that an IBR's mistuned response can be approximated as a linear combination of tuned modes [8, 12–18]. These research efforts were restricted to IBRs, while DFIBR mistuning research has been largely absent from the literature.

This effort investigates the geometric mistuning problem for DFIBRs where the use and importance of mistuned blade

modes in DFIBR ROM formulations are yet to be investigated. Mistuned blade modes were used, and shown to be important, by Beck et al. [11] for IBRs using a traditional CB-CMS reduction technique [19]. This approach is troublesome for DFIBRs since they have many more interface DOF and the resulting CB-CMS ROMs are hardly reduced. To accommodate the numerous interface DOF, a previous IBR formulation [20] is extended to DFIBRs where specific matrix operations are now needed since DFIBR blades interface with two cyclic structures. Furthermore, the use of tuned modes in a secondary modal analysis is investigated for ultimate model reduction and efficient geometric mistuning forced response prediction of DFIBRs.

This paper is organized in the following manner: first, the CB-CMS coupling procedures for DFIBR components utilizing mistuned blade modes is then given in section 2; then the new mistuning models that further reduce of the CB-CMS ROM is then described in section 3. The DFIBR test case is then illustrated in section 4 and the results of each of the mistuning models is given in section 5. Findings are then summarized in section 6.

2 Craig-Bampton Component Mode Synthesis

This study restricts mistuning to the blades and assumes nominal disk and ring geometries. By substructuring in this fashion, mistuning can be applied directly to blades so the disk and ring component matrices will be computed only once - resulting in a reduction of subsequent computational costs often incurred in Monte Carlo simulations. However, even tuned disk and ring geometries present a computational burden since they may contain the majority of the DOFs of the entire FEM. To circumvent this issue, the disk and ring are presented in a cyclic symmetry format [21] that is partitioned according to Fig. 2 for a CB-CMS approach. The component matrices of a cyclically symmetric structure are given by

$$\widetilde{\mathcal{M}} = \begin{bmatrix} I & \widetilde{\mathcal{M}}_{nc} \\ \widetilde{\mathcal{M}}_{nc}^{\mathsf{T}} & \widetilde{\mathcal{M}}_{cc} \end{bmatrix}, \widetilde{\mathcal{K}} = \begin{bmatrix} \Lambda & 0 \\ 0 & \widetilde{\mathcal{K}}_{cc} \end{bmatrix}, \widetilde{\mathcal{F}} = \begin{Bmatrix} \widetilde{\mathcal{F}}_n \\ \widetilde{\mathcal{F}}_c \end{Bmatrix} \tag{1}$$

The blade component matrices are calculated for specific blade set, i.e. Inner- or Outer-blades. Therefore, the notation *for all blades* $(\forall a)$ requires all blades be of the same set. If all blades are tuned, calculating the blade CB-CMS matrices would only have to be done once for the inner-blades and once for the outer-blades since the component matrices would be the same for all ${}^{I}N$ or ${}^{O}N$ blades. However, geometric mistuning perturbs both the mass and stiffness matrices of each inner- and outer-blade by varying amounts, e.g. $K = {}_{t}K + \Delta K$, where ${}_{t}K$ is a tuned stiffness matrix and ΔK is a perturbation matrix

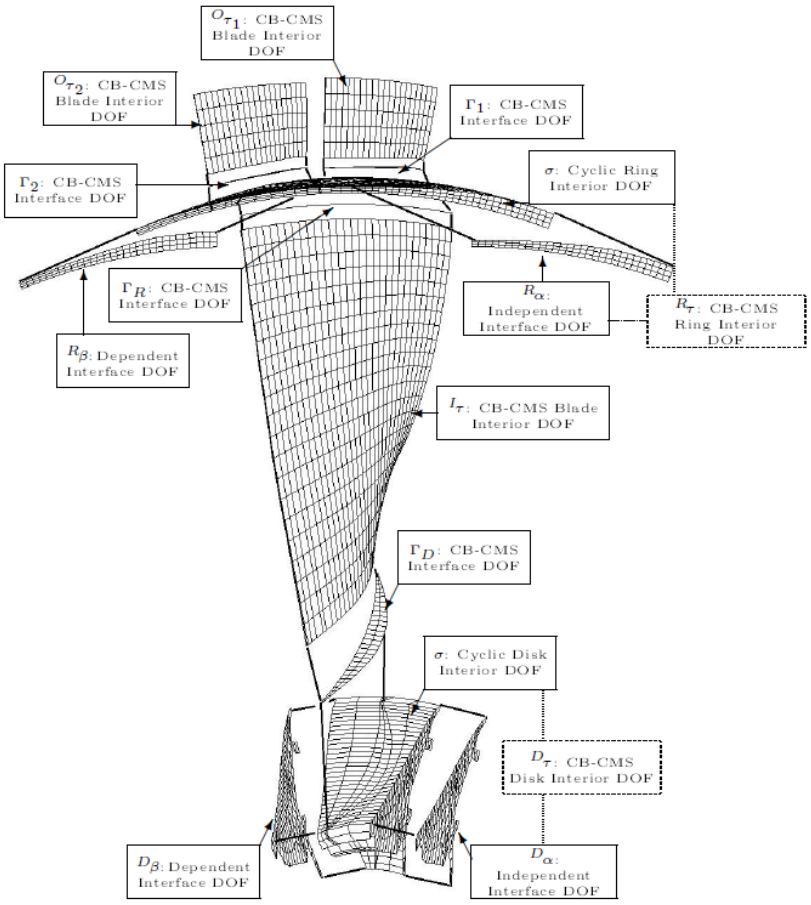

Fig. 2. Partitioned IBR index notation used in the mathematical formulation

of full rank with small deviations. Consequently, the blade matrices must be recalculated for all blades of each inner- and outer-blade set and then combined into the matrices

$$\mathcal{M} = \begin{bmatrix} I & \underset{\forall a}{\mathbb{B}}\left[\mathcal{M}_{nc}^{(a)}\right] \\ \underset{\forall a}{\mathbb{B}}\left[\mathcal{M}_{nc}^{\mathsf{T}(a)}\right] & \underset{\forall a}{\mathbb{B}}\left[\mathcal{M}_{cc}^{(a)}\right] \end{bmatrix}, \quad \mathcal{K} = \begin{bmatrix} \underset{\forall a}{\mathbb{B}}\left[\Lambda^{(a)}\right] & 0 \\ 0 & \underset{\forall a}{\mathbb{B}}\left[\mathcal{K}_{cc}^{(a)}\right] \end{bmatrix}, \quad \mathcal{F} = \begin{Bmatrix} f_n \\ f_c \end{Bmatrix} \tag{2}$$

where $\mathbb{B}$ is the block diagonal operator that places the a^{th} blade matrix on the diagonal for $a = 1, \ldots, {}^{I}N \text{ or } {}^{O}N$. The blade force vector, $\mathcal{F}$, is derived for a periodic engine order forcing function that is constant in magnitude and differs only in phase from blade-to-blade by

$$\varphi_{a,C} = \frac{2\pi C\,(a-1)}{N} \quad a = 1, \ldots, {}^{I}N \text{ or } {}^{O}N \tag{3}$$

where C is the engine order excitation for either the inner-, ${}^{I}C$, or outer-, ${}^{O}C$, blades. This type of excitation is representative of engine forcing where stationary, non-uniform pressure distributions around the annulus are felt as a harmonic load as the DFIBR rotates through the flow field. The force is assumed be constant in magnitude and differ only in phase from blade-to-blade.

2.1 Component Coupling

Previous efforts utilizing CB-CMS had specific component coupling schemes: Bladh, et al. [6] utilizes a tuned blade coupling procedure since the methodology is formulated with tuned blade modes; Beck, et al. [20] requires a modified coupling procedure from [6] since mistuned blade modes are used; and Beck, et al. [1] utilizes a tuned blade coupling procedure for tuned DFIBRs. For geometrically mistuned DFIBRs, the coupling procedure must be modified further from these efforts since mistuned blade modes are used for two different blade sets that are coupled to different subcomponents. Substructuring the DFIBR according to blade types results in the CB-CMS DOF vectors, $\mathbf{p}$, to be organized by blade type, however, they must be re-ordered according to fixed-interface normal DOF and constraint mode DOF by

$$\left\{\begin{array}{c} {}^{I}\mathbf{p}^{(\forall a)} \\ \dots \\ {}^{O}\mathbf{p}^{(\forall a)} \end{array}\right\} = \left\{\begin{array}{c} {}^{I}\mathbf{p}_n^{(\forall a)} \\ {}^{I}\mathbf{p}_c^{(\forall a)} \\ \dots \\ {}^{O}\mathbf{p}_n^{(\forall a)} \\ {}^{O}\mathbf{p}_c^{(\forall a)} \end{array}\right\} = T \left\{\begin{array}{c} {}^{I}\mathbf{p}_n^{(\forall a)} \\ {}^{O}\mathbf{p}_n^{(\forall a)} \\ \dots \\ {}^{I}\mathbf{p}_{\Gamma_D}^{(\forall a)} \\ {}^{O}\mathbf{p}_{\Gamma}^{(\forall a)} \end{array}\right\} = T \left\{\begin{array}{c} {}^{A}\mathbf{p}_n^{(\forall a)} \\ \dots \\ {}^{A}\mathbf{p}_c^{(\forall a)} \end{array}\right\} \tag{4}$$

where the left superscript, A, has been added to denote those matrices and vectors that have both inner- and outer-blade components. The transformation matrix, T, is filled with ones and zeros that allow the re-ordering of Eq. 4. The blade matrices are re-ordered with T according to

$${}^{A}\mathcal{K} = T^{\mathsf{T}} \begin{bmatrix} {}^{I}\mathcal{K} & 0 \\ 0 & {}^{O}\mathcal{K} \end{bmatrix} T = \begin{bmatrix} {}^{A}\Lambda & 0 \\ 0 & {}^{A}\mathcal{K}_{cc} \end{bmatrix}, \; {}^{A}\mathcal{M} = T^{\mathsf{T}} \begin{bmatrix} {}^{I}\mathcal{M} & 0 \\ 0 & {}^{O}\mathcal{M} \end{bmatrix} T = \begin{bmatrix} I & \mathcal{M}_{nc} \\ \mathcal{M}_{nc}^{\mathsf{T}} & {}^{A}\mathcal{M}_{cc} \end{bmatrix}, \; {}^{A}\mathcal{F} = T^{\mathsf{T}} \left\{\begin{array}{c} {}^{I}\mathcal{F} \\ {}^{O}\mathcal{F} \end{array}\right\} = \left\{\begin{array}{c} {}^{A}\mathcal{F}_n \\ {}^{A}\mathcal{F}_c \end{array}\right\} \tag{5}$$

where the inner- and outer-blade component matrices and vectors, $\mathcal{K}$, $\mathcal{M}$, and $\mathcal{F}$ are from Eq. 2.

CB-CMS model assembly requires interface displacement compatibility ${}^{I}\mathbf{x}_{\Gamma_D} = {}^{D}\mathbf{x}_{\Gamma}$ and ${}^{A}\mathbf{x}_{\Gamma} = {}^{R}\mathbf{x}_{\Gamma}$ in physical coordinates. Expanding this and utilizing the CB-CMS requirement that $\mathbf{x}_{\Gamma} = \mathbf{p}_c$ yields

$$\left\{\begin{array}{c} {}^{I}\mathbf{x}_{\Gamma_D}^{(\forall a)} \\ {}^{A}\mathbf{x}_{\Gamma}^{(\forall a)} \end{array}\right\} = \left\{\begin{array}{c} {}^{I}\mathbf{p}_{\Gamma_D}^{(\forall a)} \\ {}^{A}\mathbf{p}_{c}^{(\forall a)} \end{array}\right\} = \left[\begin{array}{cc} {}^{I}\hat{E} & 0 \\ 0 & {}^{O}\hat{E} \end{array}\right] \left\{\begin{array}{c} {}^{D}\tilde{\mathbf{p}}_{c}^{(\forall h)} \\ {}^{R}\tilde{\mathbf{p}}_{c}^{(\forall h)} \end{array}\right\} = \left\{\begin{array}{c} {}^{D}\mathbf{x}_{\Gamma} \\ {}^{R}\mathbf{x}_{\Gamma} \end{array}\right\} \tag{6}$$

where ${}^{I}\hat{E} = E \otimes {}^{I}I$, ${}^{O}\hat{E} = E \otimes {}^{O}I$, and E is the $N \times N$ real-valued Fourier matrix [6]. To constrain the blades to the disk and ring, cyclic DOF ${}^{D}\mathbf{p}_{c}^{(\forall h)}$ and ${}^{R}\mathbf{p}_{c}^{(\forall h)}$ are kept as active DOF. The resulting coupled CB-CMS ROM matrices are obtained by

$$\begin{aligned} {}^{CB}\mathcal{M} &= T^{\intercal} \left[\begin{array}{ccc} {}^{D}\widetilde{\mathcal{M}} & 0 & 0 \\ 0 & {}^{R}\widetilde{\mathcal{M}} & 0 \\ 0 & 0 & {}^{A}\mathcal{M} \end{array}\right] T = \left[\begin{array}{ccc} I & \mathcal{M}_{nc} & 0 \\ \mathcal{M}_{nc}^{\intercal} & \mathcal{M}_{cc} & {}^{A}\mathcal{M}_{nc}^{\intercal} \\ 0 & {}^{A}\mathcal{M}_{nc} & I \end{array}\right] \\ {}^{CB}\mathcal{K} &= T^{\intercal} \left[\begin{array}{ccc} {}^{D}\widetilde{\mathcal{K}} & 0 & 0 \\ 0 & {}^{R}\widetilde{\mathcal{K}} & 0 \\ 0 & 0 & {}^{A}\mathcal{K} \end{array}\right] T = \left[\begin{array}{ccc} \Lambda & 0 & 0 \\ 0 & \mathcal{K}_{cc} & 0 \\ 0 & 0 & {}^{A}\Lambda \end{array}\right] \\ {}^{CB}\mathcal{F} &= T^{\intercal} \left\{\begin{array}{c} {}^{D}\widetilde{\mathcal{F}} \\ {}^{R}\widetilde{\mathcal{F}} \\ {}^{A}\mathcal{F} \end{array}\right\} = \left\{\begin{array}{c} \widetilde{\mathcal{F}}_n \\ \mathcal{F}_c \\ {}^{A}\mathcal{F}_n \end{array}\right\} \end{aligned} \tag{7}$$

where T is the coupling matrix composed of ones, zeros, and real-valued Fourier matrices.

When all the blades are tuned, the cyclic DOF ${}^{D}\tilde{\mathbf{p}}_{c}^{(\forall h)}$ and ${}^{R}\tilde{\mathbf{p}}_{c}^{(\forall h)}$ are kept as active DOF when constraining the blades to the disk and ring. This keeps portions of the CB-CMS matrices in cyclic format that allows faster calculation of secondary eigenvalue problems (EVPs) outlined in Section 3. The cyclic versions of the constraint DOF partitions to Eq. 7 are

$$\widetilde{\mathcal{M}}_{nc} = \left[\begin{array}{cc} {}^{D}\widetilde{\mathcal{M}}_{nc} & 0 \\ 0 & {}^{R}\widetilde{\mathcal{M}}_{nc} \end{array}\right], \quad \widetilde{\mathcal{M}}_{cc} = \left[\begin{array}{cc} {}^{D}\widetilde{\mathcal{M}}_{cc} + {}^{I}\hat{E}^{\intercal}{}_{t}^{A}\mathcal{M}_{\Gamma_D\Gamma_D}{}^{I}\hat{E} & {}^{I}\hat{E}^{\intercal}{}^{A}\mathcal{M}_{\Gamma_D\Gamma}{}^{O}\hat{E} \\ {}^{O}\hat{E}^{\intercal}{}_{t}^{A}\mathcal{M}_{\Gamma_D\Gamma}^{\intercal}{}^{I}\hat{E} & {}^{R}\widetilde{\mathcal{M}}_{cc} + {}^{O}\hat{E}^{\intercal}{}_{t}^{A}\mathcal{M}_{\Gamma\Gamma}{}^{O}\hat{E} \end{array}\right] \tag{8}$$

where $\widetilde{\mathcal{K}}_{cc}$ follows the same partitionment as $\widetilde{\mathcal{M}}_{cc}$

2.2 CB-CMS ROM

The CB-CMS EOM is formulated from Eq. 7 as

$$ {}^{CB}\mathcal{M}\ddot{\mathbf{p}} + {}^{CB}\mathcal{C}\dot{\mathbf{p}} + (1+\mathcal{G}\mathrm{i})\,{}^{CB}\mathcal{K}\mathbf{p} = {}^{CB}\mathcal{F} \tag{9} $$

where the damping matrix and structural damping coefficient, ${}^{CB}\mathcal{C}$ and $\mathcal{G}$, respectively, have can be included to better model dynamic response [6]. The damping matrix ${}^{CB}\mathcal{C}$ can have a submatrices of blade modal damping matrices

$$ {}^{A}\mathcal{C} = \begin{bmatrix} \underset{\forall a}{\mathbb{B}}\left[\mathrm{diag}\left(2\,{}^{I}\zeta_j^{(a)}\right)\sqrt{{}^{I}\Lambda^{(a)}}\right] & 0 \\ 0 & \underset{\forall a}{\mathbb{B}}\left[\mathrm{diag}\left(2\,{}^{O}\zeta_j^{(a)}\right)\sqrt{{}^{O}\Lambda^{(a)}}\right] \end{bmatrix} \tag{10} $$

where ζ_j is the damping coefficient for the j^{th} blade mode. This CB-CMS model is dominated by the unnecessary retention of all the interface DOF and, at times, the disk and ring normal DOF. The following sections seek to further reduce the size of this CB-CMS ROM by performing a secodary modal analysis on this model.

3 Secondary Modal Reduction ROMs

The CB-CMS model of Eq. 9 requires retention of all constraint DOF. For DFIBRs with a large inner- and outer-blade count, the ROM will be dominated by the interface DOF that prevent an ultimate reduction in model size. To reduce this burden, a secondary eigen-analysis can be performed on portions of the CB-CMS system matrices that will re-cast these portions into a new modal domain. Two approaches are performed in this work: first, the secondary eigen-analysis is carried out on the constraint DOF partitions of the CB-CMS system matrices. The resulting truncated set of eigenvectors yield a set of interface modes. The second approach performs an eigen-analysis on the constraint and disk and ring fixed-interface normal mode DOF partitions. The resulting truncated set of eigenvectors are termed ancillary modes. The cyclic formulation offers computational savings by carrying out the analysis in cyclic coordinates which allows each harmonic index to be solved independently.

In the following subsections, two mistuning approaches are presented that use either the tuned interface or ancillary

modes to further reduce the CB-CMS ROM size of Eq. 9. In both approaches, the generic equation of motion (EOM) is given by

$$M_r\ddot{\mathbf{q}}_r + C_r\dot{\mathbf{q}}_r + (1+G\mathrm{i})\,K_r\mathbf{q}_r = \mathbf{F}_r \tag{11}$$

where subscript r refers to *reduced* and the EOM matrices are defined in the following subsections. These two models are compared to a traditional tuned blade mode approximation that is formulated in a previous effort [1].

3.1 Interface Mode Reduction

The tuned blade CB-CMS matrices keep the constraint DOF in cyclic coordinates that allows the constraint modes to be calculated at decoupled harmonics, following a matrix reordering described in [1]. This gives the constraint DOF matrices $\widetilde{\mathcal{M}}_{cc}^{(\text{h-ord})}$ and $\widetilde{\mathcal{K}}_{cc}^{(\text{h-ord})}$, where the superscript (h-ord) reminds that it is ordered by harmonic indices. These matrices have a block-diagonal structure, where the h^{th} block corresponds to the constraint DOF symmetrical components of the h^{th} harmonic. The interface mode shapes can then calculated one harmonic at a time by the EVP of $\widetilde{\mathcal{M}}_{cc}^{(\text{h-ord})}$ and $\widetilde{\mathcal{K}}_{cc}^{(\text{h-ord})}$, for $k_{cc} \ll N_{\Gamma_D} + N_\Gamma$ modes at each harmonic. The interface modes are assembled into the modal matrix $\tilde{\Phi}_{cc}^{(h)} = \left[\tilde{\phi}_1, \ldots, \tilde{\phi}_{k_{cc}}\right]$ and then combined for all harmonics and transformed back to physical space by

$$\Phi_{cc} = \hat{E}T_1 \mathop{\mathbb{B}}_{\forall h}\left[\tilde{\Phi}_{cc}^{(h)}\right] \tag{12}$$

where $\hat{E} = \mathbb{B}\left({}^{I}\hat{E}, {}^{O}\hat{E}\right)$ and T_1 is a boolean matrix that created the h-ord matrices. Since a limited set of k_{cc} tuned interface modes is retained, the CB-CMS system of Eq. 9 can be further reduced through the following transformation matrix

$${}^{CB}\mathbf{p} = \begin{bmatrix} I & 0 & 0 \\ 0 & \Phi_{cc} & 0 \\ 0 & 0 & I \end{bmatrix} \begin{Bmatrix} \tilde{\mathbf{q}}_n \\ \mathbf{q}_c \\ {}^{A}\mathbf{q}_n \end{Bmatrix} = T_{CC}\mathbf{q}_r \tag{13}$$

Substituting this into the CB-CMS EOM of Eq. 9 and pre-multiplying by T_{CC}^{T} yields the following matrices for the reduced ROM of Eq. 11

$$\mathcal{M}_r = \begin{bmatrix} I & \mathcal{M}_{nc}\tilde{\Phi}_{cc} & 0 \\ \Phi_{cc}^{\mathsf{T}}\mathcal{M}_{nc}^{\mathsf{T}} & \Phi_{cc}^{\mathsf{T}}\mathcal{M}_{cc}\Phi_{cc} & \Phi_{cc}^{\mathsf{T}}{}^{A}\mathcal{M}_{nc}^{\mathsf{T}} \\ 0 & {}^{A}\mathcal{M}_{nc}\Phi_{cc} & I \end{bmatrix}, \mathcal{K}_r = \begin{bmatrix} \Lambda & 0 & 0 \\ 0 & \Phi_{cc}^{\mathsf{T}}\mathcal{K}_{cc}\Phi_{cc} & 0 \\ 0 & 0 & {}^{A}\Lambda \end{bmatrix}, \mathcal{F}_r = \begin{Bmatrix} \widetilde{\mathcal{F}}_n \\ \Phi_{cc}^{\mathsf{T}}\mathcal{F}_c \\ {}^{A}\mathcal{F}_n \end{Bmatrix}$$

Note that C_r is obtained in the same manner, except only the size of the disk and ring entries are changed, so it is not re-listed.

Mistuned interface modes in physical space can also be utilized for reduction of the CB-CMS ROM, but do not provide any subsequent computational savings. However, it results in a ROM of the same size that is a fair comparison for the tuned interface reduction procedure. A subset of mistuned interface modes is then combined into the mistuned interface modal matrix $\Phi_{cc} = \left[\phi_1, \ldots, \phi_{k_{cc}}\right]$. This set of modes is then substituted into Eq. 13 to provide a mistuned interface mode reduction.

3.2 Ancillary Mode Reduction

The disk and ring components are tuned so the normal DOF pertaining to these substructures remain unchanged from one mistuned DFIBR to the next. Therefore, the cyclic constraint partitions and disk and ring normal partitions can be re-ordered by harmonics to yield a block-diagonal structure that allows the computational benefits of cyclic symmetry. This re-ordering by harmonics is done according to

$$\tilde{\mathbf{p}}^{(\forall h)} = \begin{Bmatrix} {}^{D}\tilde{\mathbf{p}}_n^{(\forall h)} \\ {}^{R}\tilde{\mathbf{p}}_n^{(\forall h)} \\ {}^{D}\tilde{\mathbf{p}}_c^{(\forall h)} \\ {}^{R}\tilde{\mathbf{p}}_c^{(\forall h)} \end{Bmatrix} = T_2 \begin{Bmatrix} \tilde{\mathbf{p}}_s^{(1)} \\ \vdots \\ \tilde{\mathbf{p}}_s^{(N/2)} \end{Bmatrix} = T_2 \tilde{\mathbf{p}}_s^{(\text{h-ord})} \tag{14}$$

where $\tilde{\mathbf{p}}_s^{(h)} = \left[{}^{D}\tilde{\mathbf{p}}_n^{(h)} \; {}^{R}\tilde{\mathbf{p}}_n^{(h)} \; {}^{D}\tilde{\mathbf{p}}_c^{(h)} \; {}^{R}\tilde{\mathbf{p}}_c^{(h)} \right]^{\mathsf{T}}$ and T_2 is a Boolean matrix. The corresponding block-diagonal, harmonic-ordered matrices are obtained by

$$\widetilde{\mathcal{M}}_{ss} = \mathop{\mathbb{B}}_{\forall h}\left[\widetilde{\mathcal{M}}_{ss}^{(h)}\right] = T_2^{\mathsf{T}} \begin{bmatrix} I & \widetilde{\mathcal{M}}_{nc} \\ \widetilde{\mathcal{M}}_{nc}^{\mathsf{T}} & \widetilde{\mathcal{M}}_{cc} \end{bmatrix} T_2, \quad \widetilde{\mathcal{K}}_{ss} = \mathop{\mathbb{B}}_{\forall h}\left[\widetilde{\mathcal{K}}_{ss}^{(h)}\right] = T_2^{\mathsf{T}} \begin{bmatrix} \Lambda & 0 \\ 0 & \widetilde{\mathcal{K}}_{cc} \end{bmatrix} T_2 \tag{15}$$

The ancillary mode shapes can then be calculated one harmonic at a time by the following EVP of $\widetilde{\mathcal{K}}_{ss}^{(h)}$ and $\widetilde{\mathcal{M}}_{ss}^{(h)}$ for $k_{ss} \ll {}^{D}k_n + {}^{R}k_n + N_{\Gamma_D} + N_{\Gamma}$ modes, where the ancillary modes are assembled into the modal matrix $\tilde{\Phi}_{ss}^{(h)} = \left[\tilde{\phi}_1, \ldots, \tilde{\phi}_{k_{ss}}\right]$ and then combined for all harmonics by

$$\Phi_{ss} = V T_2 \mathop{\mathbb{B}}_{\forall h}\left[\tilde{\Phi}_{ss}^{(h)}\right] \tag{16}$$

where $V = \mathbb{B}\left(I, {}^{I}\hat{E}, {}^{O}\hat{E}\right)$. Since a limited set of k_{ss} tuned ancillary modes is retained at each harmonic, the CB-CMS system can be further reduced through the following transformation matrix

$${}^{CB}\mathbf{p} = \begin{bmatrix} \Phi_{ss} & 0 \\ 0 & I \end{bmatrix} \begin{Bmatrix} \mathbf{q}_s \\ {}^{A}\mathbf{p}_n \end{Bmatrix} = T_{CA}\mathbf{q}_r \tag{17}$$

Substituting this into the CB-CMS EOM of Eq. 9 and pre-multiplying by T_{CA}^{T} yields the following matrices for the reduced ROM of Eq. 11

$$\mathcal{M}_r = T_{CA}^{\mathsf{T}}\,{}^{CB}\mathcal{M}T_{CA}, \quad \mathcal{K}_r = T_{CA}^{\mathsf{T}}\,{}^{CB}\mathcal{K}T_{CA}, \quad \mathcal{F}_r = T_{CA}^{\mathsf{T}}\,{}^{CB}\mathcal{F} \tag{18}$$

As in the case of interface mode reduction, only the size of the disk and ring entries in C_r are changed, so it is not re-listed. Furthermore, a subset of mistuned ancillary modes can combined into the modal matrix $\Phi_{ss} = \left[\phi_1, \ldots, \phi_{k_{ss}}\right]$ and then substituted into Eq. 17 to provide a mistuned ancillary mode reduction.

Table 1. Mistuning ROM sizes

Models	Size Eq.
CB-CMS	${}^{I}N\left({}^{D}k_n + {}^{R}k_n + {}^{I}k_n + N_{\Gamma_D} + N_{\Gamma}\right) + {}^{O}N^{O}k_n$
Interface (CC)-Reduced	${}^{I}N\left({}^{D}k_n + {}^{R}k_n + {}^{I}k_n\right) + {}^{O}N^{O}k_n + k_{cc}$
Ancillary (CA)-Reduced	${}^{I}N^{I}k_n + {}^{O}N^{O}k_n + k_{ca}$

3.3 Method Comparison

The CB-CMS method is formulated from mistuned blade matrices and mistuned blade CB-CMS transformation matrices. This CB-CMS model is then reduced using an interface mode reduction (CC) with either a tuned (T) or mistuned (M) interface modes. These methods are referred to as CCT and CCM, respectively, for the results comparison. The CB-CMS model is also reduced using an ancillary mode reduction (CA) with either a tuned (T) or mistuned (M) ancillary modes. These methods are referred to as CAT and CAM, respectively. The last method, CCN, is a tuned interface mode reduction of a CB-CMS matrix formulated with tuned components which is then mistuned by introducing the inner- and outer-blade frequencies from the geometrically perturbed DFIBR. The N serves as a reminder that this method uses nominal, or tuned, blade modes in the reduction/expansion for mistuned DFIBRs. This is a frequency-based approach developed in [1] and is analogous to frequency-based approaches for IBRs widely used in academia and industry. This CCN method assumes blade geometric perturbations alter only the corresponding modal stiffnesses while its mode shapes remain unaffected.

Table 1 outlines the size governing equation of each ROM discussed as a function of the number of blades and truncated modes retained in each method's formulation. As previously outlined, the traditional CB-CMS ROM is the largest of these approaches and its size can be prohibitively large as the number of interface DOF increases. The remaining CC- and CA-reduced methods outlined in Sections 3.1 and 3.2 seek to further reduce the size of the CB-CMS method. The CA-reduced model sizes are independent of ${}^{D}k_n$ and ${}^{R}k_n$ since this reduction method includes the disk and ring fixed interface modes in the secondary modal analysis. Increasing ${}^{D}k_n$ and ${}^{R}k_n$ has the benefit of increasing the accuracy of the ancillary mode reduction method without increasing the ROM size. However, this increase comes at the computational cost of calculating the ancillary modes in a larger EVP.

As the number of fixed interface normal modes retained for all components approaches their respective maximum, the prediction converges to the full FEM as the number of retained mistuned interface and ancillary modes approach their respective maximum. However, as these limits are approached, the ROM can hardly be called reduced. Note that convergence to the full FEM solution is only true when using mistuned blade, interface and ancillary modes since the tuned mode reduction methods are approximations.

Table 2. Basic FEM size data for the DFIBR partitioning defined in Fig. 2

Component	Nodes	DOF
${}^{D}\tau$	813	2439
${}^{R}\tau$	1714	5142
${}^{I}\tau$	1240	3720
${}^{O}\tau$	252	756
$\Gamma_R + \Gamma_D$	124	373
Γ_i	42	126
Full Model	28704	86112

4 Test Case

The DFIBR used in this study has ${}^{I}N = 16$ inner-blades and ${}^{O}N = 32$ outer-blades. The outer-blades are circumferentially offset from inner-blades by a fourth of the inter blade phase angle of the DFIBR. The FEM is meshed with eight-node linear hexahedral elements with translations in the x-, y-, and z-directions at each node. The mesh density is listed in Table 2 is used for all mistuning prediction methods. The disk is constrained to zero displacements in all three directions at the hub. Mistuning is implemented through perturbations to the blade surfaces. These geometric deviations are measured from a different industrial turbine engine fan using a coordinate measurement machine. These deviations are first reduced using Principal Component Analysis and then mapped onto the inner- and outer- blade surfaces. New deviations are introduced through perturbations to a blade's Principal Component features that quantify small geometrical variations in a blade's geometry [22–24] that result in non-proportional frequency perturbations.

A nodal diameter (ND) plot illustrating the tuned system natural frequencies versus the harmonic index is shown in Fig. 3. This plot characterizes the free vibration of the DFIBR by highlighting regions consisting of system modes and those of mainly blade motion. Veering regions contain system modes that offer significant interaction between the motion of the blades, disk, and ring [1]. The nearly horizontal portions of each mode family consist primarily of blade motion. In DFIBRs, there are two sets of blades of different geometries that will now characterize the mode family. In fact, it is shown that the primarily flat regions consist of either an inner- (outer-) blade mode type and then transition to an outer- (inner-) blade mode type through the slanted, or system mode regions of the ND plot. Furthermore, while the inner-blades are essentially subject to fixed-fixed boundary conditions at the blade root and tip, inner-blade motions will can still resemble a cantilevered-blade motion for certain mode families.

5 Results

Results are generated for a geometrically mistuned DFIBR by perturbing the PCs that describe the geometry deviations of the blade surface. The DFIBR is subject to the EO excitations ${}^{I}C = {}^{O}C = 0$ over an excitation frequency range of $1450 -$

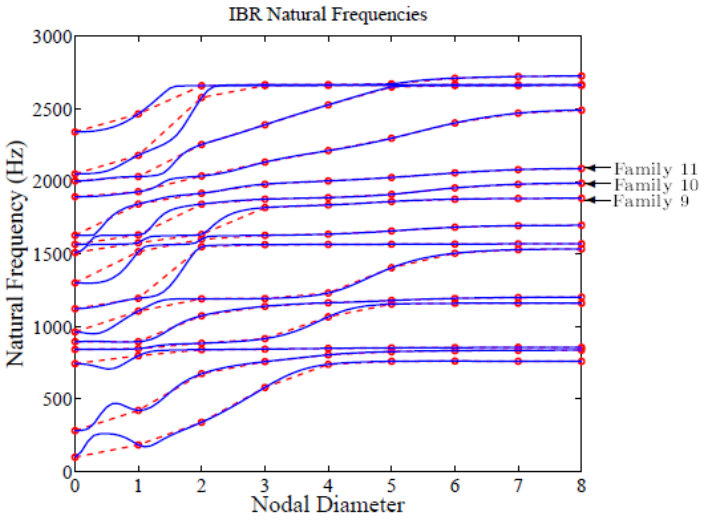

Fig. 3. The nodal diameter plot of the DFIBR illustrating the tuned system natural frequencies versus the harmonic index

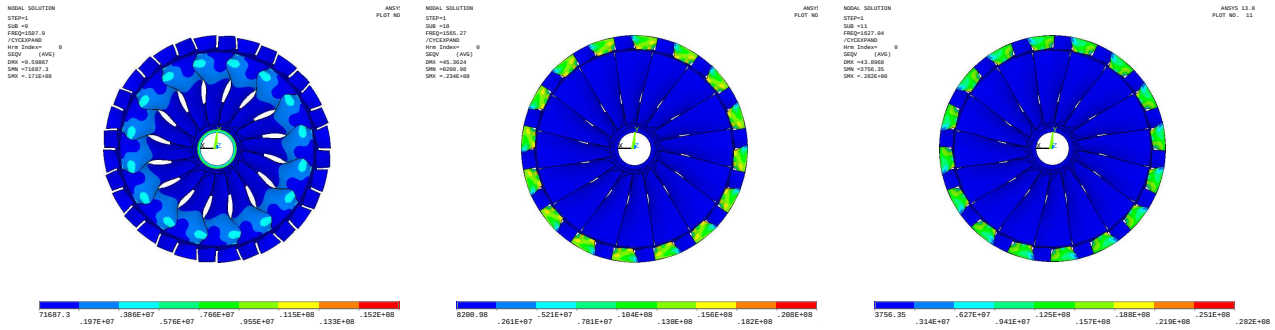

(a) System Mode 98 (b) System Mode 110 (c) System Mode 122

Fig. 4. Tuned DFIBR system modes in the frequency range of interest at harmonic index $h = 0$

$1750\,Hz$. These conditions will excite tuned system modes 98, 110, and 122 of mode families 9, 10, and 11, respectfully, at harmonic index $h = 0$ of Fig. 3. These modes are depicted in Fig. 4, where mode 98 in Fig. 4(a) is primarily inner-blade fixed-fixed blade torsion motion while modes 110 and 122 are primarily cantilevered blade torsion motion. This DFIBR exhibits response amplification and is a good test case for the developed methods since it will demonstrate the ability to predict the magnification. Capturing this phenomenon is critical for accurate life assessment by ensuring that peak response does not exceed a predetermined critical value.

For this study, a unit force is applied to a single location on the outer-blade trailing edge tips and inner-blades at mid-span. While not representative of in-flight loading, this type of forcing can demonstrate the mistuning phenomenon and is usually prescribed in bench-level testing. The response levels are "measured" at a single output location on the leading edge of outer-blade tips and inner-blades at mid-span. These input/output locations were determined by upfront studies that identified blade locations that were easiest to elicit a response.

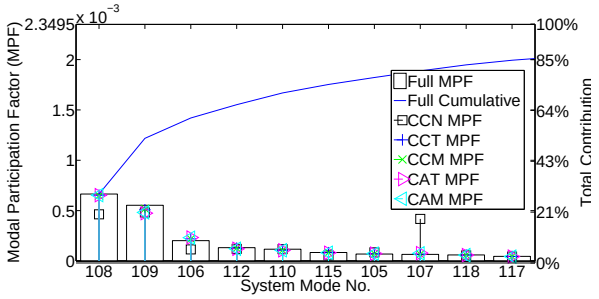

Fig. 5. Modal participation factors for the EO excitations ${}^{I}C = {}^{O}C = 0$ over an excitation frequency range of $1450 - 1750\,Hz$.

In the sections that follow each ROM is compared against a full FEM solution obtained from the commercially available ANSYS software. The best achievable ROM results will belong to those predicted by the mistuned formulation of the traditional CB-CMS approach (labeled CMS in the following figures), since it is formulated with mistuned component matrices and modes while retaining all constraint DOF. The mistuned ancillary and interface mode reduction methods (labeled CCM and CAM in the following figures) will approach the accuracy of CB-CMS since these methods are synthesized from this parent model using mistuned modes in the reduction process. The accuracy of the tuned ancillary and interface mode reduction methods (labeled CCT and CAT in the following figures), should follow suit, depending how accurate the assumption that the tuned modes span the same space as the mistuned modes. In the results that follow, CCT and CAT are always compared against their mistuned mode counterpart, CCM and CAM, respectively, since the latter methods make no approximations other than modal truncations. Accuracy of calculated system modes and modal participation factors (MPF) are first discussed in Section 5.1. These values directly contribute to accuracy of blade-to-blade and peak DFIBR forced responses, discussed in Sections 5.2 and 5.3, respectively. Finally, model size and computation time comparisons are made in Subsection 5.4.

5.1 Modal Participations

A subset of predicted system mode shapes are chosen for comparison in this section. For the excitation conditions of interest, the modal participation factors are determined for a modal summation response and are shown in the Pareto plot of Fig. 5. The first ten modes with the highest modal participation are plotted on the abscissa. The bars and stems corresponding to the left ordinate illustrate the modal contributions of each ROM. As illustrated, CCN incorrectly identifies the modes with the largest participation factors and the amount these modes participate, e.g. mode 107 is incorrectly identified by CNN as participating a significant amount to the forced response. Large errors for the first ten modes will have a negative impact on predicted forced response levels, since these modes contribute to more than 85% of all the modes in the forced response levels, as illustrated by the line plot corresponding to the right ordinate.

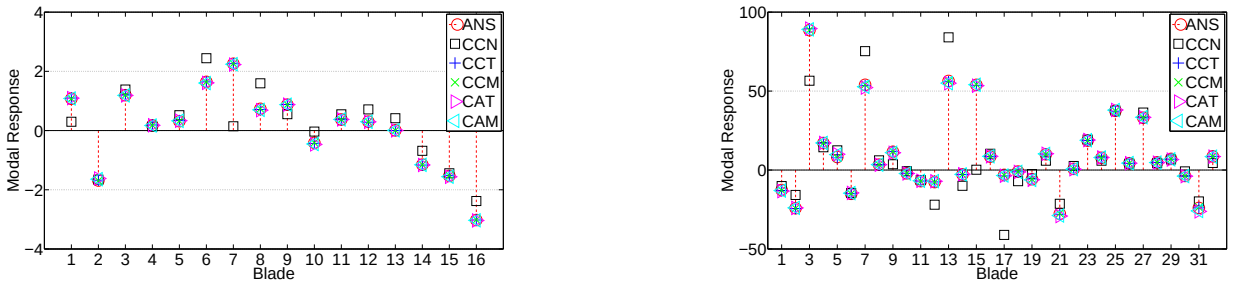

(a) Inner-Blades (b) Outer-Blades

Fig. 6. Comparison of predicted mistuned mode 109 against the full FEM solution

Mistuned IBR mode 109 is shown to have the second largest modal contribution to the forced response and is shown in the stem plots of Fig. 6 for the inner- and outer blades. In each subfigure, the modal response in the z-direction at the blade output locations are plotted for each blade around the DFIBR for a respective ROM and the full FEM prediction. The CMS method has the highest accuracy, as expected, and is shown to be in very good agreement with the full FEM. CCT and CCM also show good agreement between each ROM and the full FEM. Slight errors on select blades can be reduced by increasing the number of retained interface modes. There is also good agreement between CCT and CCM, which provides an indicator that the tuned interface modes method provide an accurate reduction method. Similar results are obtained for CAT and CAM. The CCN ROM accuracy diminishes greatly for a majority of the inner- and outer-blades. It is shown later that this error in conjunction with error in the modal participation factor manifests in larger errors in forced response levels.

5.2 Blade-to-Blade Responses

Calculated blade responses correspond to the euclidean distance of displacements over the excitation frequency range. Blade-to-blade responses represent a conservative case in assuming that blades experience this forced response level over the entire excitation frequency range, but provides a better assessment of the responses (stresses) that each blade experiences. Figure 7(a) illustrates a stem plot of CMS and CCN predicted response levels at the previously described output locations on each blade. Both the inner- and outer-blades are plotted circumferentially around the DFIBR on the abscissa, but only the inner blades ($I1-I16$) are numbered. After each inner-blade, the two outer-blades that follow before the next inner-blade are shown with simple tick marks. The forced response levels of the ordinate have been normalized by the blades' corresponding tuned response levels, so mistuned response amplification will then appear larger than one. This test case exhibits strong mistuned response amplification for the inner-blades since seven of the 16 inner-blades are responding above $2x$ the tuned prediction with the largest $3.7x$ belonging to inner-blade #2 (I2).

The CMS predictions are shown since this represents the best attainable since the only approximation in this formulation is the truncation of component fixed-interface modes. Also depicted are the CCN predictions that have large errors on certain

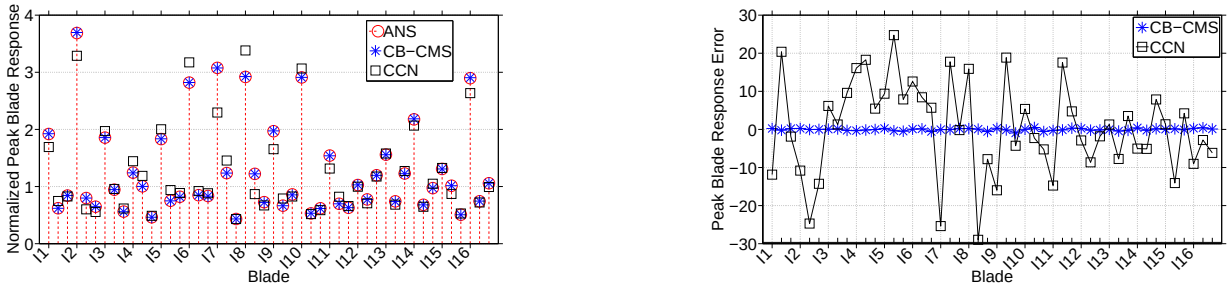

(a) Forced Response (b) Blade-to-Blade Error

Fig. 7. CCN and CMS blade-to-blade forced response predictions for the mistuned DFIBR compared against full FEM solutions

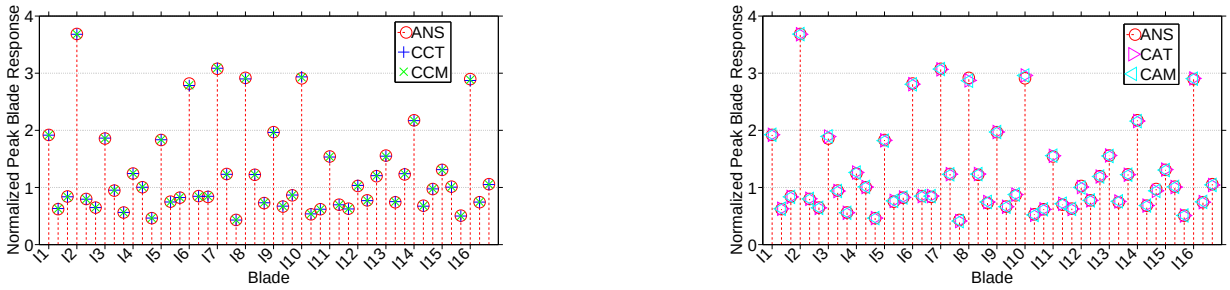

(a) CCT and CCM (b) CAT and CAM

Fig. 8. Interface (CC) and ancillary (CA) reduced ROMs' blade-to-blade forced response predictions for the mistuned DFIBR compared against full FEM solutions

blades. This manifests from the method's inability to accurately predict the system modes and modal participation factors previously discussed. Figure 7(b) plots the percent error between the ROM predictions and the full FEM results. It is clear from this picture that there are instances where the tuned mode approximation method, CCN, has large errors.

The CCT and CCM blade-to-blade predictions are shown in Fig. 8(a) and show improvement over the CCN predictions. Similar results are also obtained for both CAT and CAM. Both approaches that use mistuned modes in the reduction process give an indication if enough interface or ancillary modes are retained since they will approach the CMS solution. The percent error of each blade response as compared to the full FEM solution is shown in Fig. 9. The errors of both CC- and CA- methods compare well to the errors of the CMS approach, with the largest belonging to the CA- ROMs. Of particular importance is how closely the error of tuned mode reductions methods, CCT and CAT, follows their mistuned counterparts, CCM and CAM. In some cases, the errors are almost identical. This evidence suggests that using the tuned mode approximations for both methods introduces minor errors beyond what is already inherent in the models. Furthermore, since CCM and CAM will approach the CMS solution, this closeness of errors suggests that simply increasing the number of retained interface or ancillary modes will provide even greater accuracy.

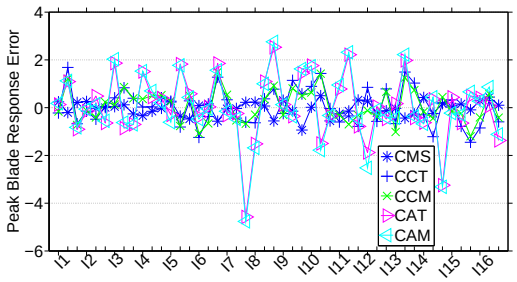

Fig. 9. Interface (CC) and ancillary (CA) reduced ROMs' blade-to-blade forced response prediction error for the mistuned DFIBR compared against full FEM solutions

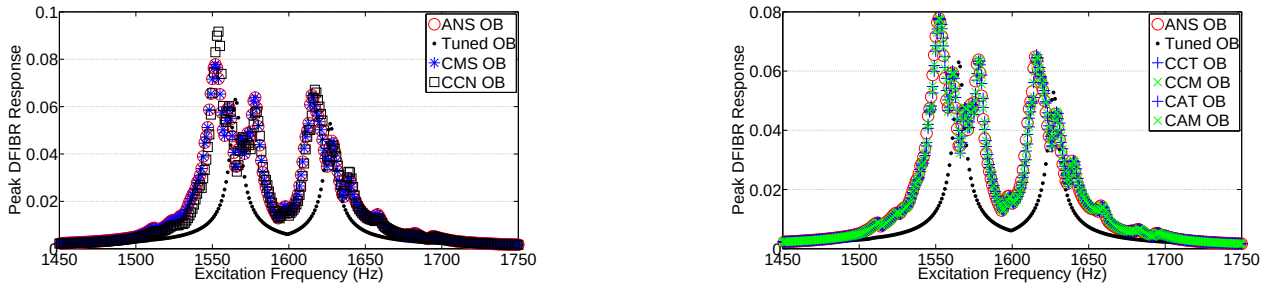

(a) CMS and CCN

(b) CC- and CA- Methods

Fig. 10. ROM peak DFIBR forced response predictions of the inner-blades as compared to the full FEM solution

5.3 Peak DFIBR Responses

Peak DFIBR response is the maximum mistuned response seen on the DFIBR and represents the worst case, and conservative, scenario that all blades are experiencing this response level. Figure 10 illustrates the predicted peak DFIBR mistuned response for all methods for the outer-blades only. The CCN prediction in Fig. 10(a) over predicts that actual response levels with 17.8% error. On the higher responding inner-blades the CCN method under-predicts the peak response with an error of 8.3%. The remaining CC- and CA ROMs of Fig. 10(b) all capture the peak response quite well. For all cases the error was less than 1%, providing further evidence that the tuned interface and ancillary mode reduction methods do not introduce significant errors.

5.4 Model Sizes and Solution Times

The values that determine the model sizes from Table 1 are listed in Table 3. The resulting model sizes in Table 4 have been normalized by the size of the full FEM and show that the developed interface and ancillary modal reduction methods can attain a signifacntly smaller ROM. This smaller size is beneficial to solution of the the EVP of each ROM. The ROM EVP solution times are calculated using Matlab's tic/toc function are also listed in Table 4 and have been normalized by the full FEM EVP solution time. As shown, a drawback of the CB-CMS approach is the ROM EVP can take longer to solve than the full FEM. This is due to the fully-populated constraint DOF portion of the matrices that causes significant

Table 3. Developed ROM sizes

	CB-CMS	Int-Red	Anc-Red
${}^{D}k_n$	5	5	5
${}^{R}k_n$	5	5	5
${}^{I}k_n$	30	30	30
${}^{O}k_n$	30	30	30
N_{Γ_D}	186	n/a	n/a
N_{Γ}	438	n/a	n/a
k_{cc}	n/a	250	n/a
k_{ca}	n/a	n/a	250

Table 4. Developed ROM Size Comparisons

Model	Normalized Size	Normalized Solution Time
CB-CMS	0.155	1.202
Int-Red	0.043	0.039
Anc-Red	0.037	0.037

burden to sparse eigen-solvers. Sparsity is kept intact for the full FEM and allows faster computation. However, the CB-CMS approach allows direct access to blade natural for intentional mistuning studies without regenerating a full FEM. The interface and ancillary reduction methods are necessary for obtaining a ROM that is smaller with a computationally tractable EVP. The formulation of the interface and ancillary ROMs require the additional computational expense of a secondary EVP, however, using tuned modes requires this expense only once as an upfront requirement. Furthermore, this secondary EVP is calculated in cyclic coordinates that greatly reduces the computational expenses. While the interface mode and ancillary mode reduction methods result in similar accuracy, size, and solution time, the ancillary mode method has the benefit of being of having better accuracy when increasing the number of disk and ring normal modes without increasing the overall ROM model size.

6 Conclusions

Two geometric mistuning approaches are advanced for DFIBRs by performing a secondary modal analysis on different submatrices of a parent CB-CMS ROM formulated in cyclic coordinates. A tuned disk and ring are assumed with geometric perturbations contained to inner- and outer-blades. The first method computes the interface modes of the CB-CMS constraint DOF while the second method computes ancillary modes of the constraint and disk and ring fixed interface normal modes. These modes could be either tuned or mistuned. The tuned modes are calculated in cyclic coordinates that offer significant computation savings, while the mistuned modes eliminate the approximation of using tuned modes in the reduction process. It should be noted, however, that reducing the parent ROM with mistuned interface and ancillary modes for subsequent

analyses is not prudent since the modes have to be recalculated for each mistuned configuration. Free and forced response results of ROM using both tuned and mistuned secondary modal reductions highlight that this is an accurate approximation for the given test case. Furthermore, the geometric mistuning methods are shown to have higher accuracy for peak DFIBR response and blade-to-blade predictions than a frequency-based approach. The geometric mistuning methods are also shown to have a significant reduction in solution time of the eigen-problem from the traditional CB-CMS ROM.

References

[1] Beck, J., Slater, J. C., Brown, J. M., and Cross, C. J., "Dynamic Response Characteristics of Dual Flow-Path Integrally Bladed Rotors," *AIAA SciTech*, American Institute of Aeronautics and Astronautics, Jan. 2014, pp. –.

[2] Castanier, M., Ottarsson, G., and Pierre, C., "A Reduced order modeling technique for mistuned bladed disks," *Journal of Vibration and Acoustics, Transactions of the ASME*, Vol. 119, No. 3, 1997, pp. 439 – 447.

[3] Yang, M.-T. and Griffin, J., "A reduced-order model of mistuning using a subset of nominal system modes," *ASME J Gas Turb Pwr*, Vol. 123, No. 4, 2001, pp. 893 – 900.

[4] Yang, M.-T. and Griffin, J. H., "A Reduced Order Approach for the Vibration of Mistuned Bladed Disk Assemblies," *ASME J Gas Turb Pwr*, Vol. 119, No. 1, 1997, pp. 161–167.

[5] Feiner, D. and Griffin, J., "A fundamental model of mistuning for a single family of modes," *ASME J Turbomach*, Vol. 124, No. 4, 2002, pp. 597 – 605.

[6] Bladh, R., Castanier, M. P., and Pierre, C., "Component-mode-based reduced order modeling techniques for mistuned bladed disks-Part 1: Theoretical models," *ASME J Gas Turb Pwr*, Vol. 123, No. 1, 2001, pp. 89 – 99.

[7] Vargiu, P., Firrone, C., Zucca, S., and Gola, M., "A reduced order model based on sector mistuning for the dynamic analysis of mistuned bladed disks," *International Journal of Mechanical Sciences*, Vol. 53, No. 8, 2011, pp. 639 – 646.

[8] Lim, S.-H., Bladh, R., Castanier, M., and Pierre, C., "Compact, generalized component mode mistuning representation for modeling bladed disk vibration," *AIAA Journal*, Vol. 45, No. 9, Sept. 2007, pp. 2285 – 98.

[9] Tran, D.-M., "Component mode synthesis methods using partial interface modes: Application to tuned and mistuned structures with cyclic symmetry," *Computers and Structures*, Vol. 87, No. 17-18, 2009, pp. 1141 – 1153.

[10] Yang, M.-T. and Griffin, J., "Normalized modal eigenvalue approach for resolving modal interaction," *ASME J Gas Turb Pwr*, Vol. 119, No. 3, 1997, pp. 647 – 650.

[11] Beck, J. A., Brown, J. M., Slater, J. C., and Cross, C. J., "Probabilistic mistuning assessment using nominal and geometry based mistuning methods," *Proceedings of the ASME Turbo Expo*, Copenhagen, DEN, 2012, pp. 1–13.

[12] Lim, S.-H., Castanier, M., and Pierre, C., "Vibration modeling of bladed disks subject to geometric mistuning and design changes," *Proceedings of the 45th AIAA/ASME/ASCE/AHS/ASC Structures, Structural Dynamics and Materials Conference*, Palm Springs, CA, USA, 2004.

[13] Petrov, E., Sanliturk, K., and Ewins, D., "A new method for dynamic analysis of mistuned bladed disks based on the exact relationship between tuned and mistuned systems," *ASME J Gas Turb Pwr*, Vol. 124, No. 3, 2002, pp. 586 – 597.

[14] Brown, J. M., *Reduced Order Modeling Methods for Turbomachinery Design*, Ph.D. thesis, Wright State University, Dayton, OH, 2009.

[15] Sinha, A., "Reduced-Order Model of a Bladed Rotor With Geometric Mistuning," *ASME J Turbomach*, Vol. 131, No. 3, 2009, pp. 031007.

[16] Bhartiya, Y. and Sinha, A., "Reduced Order Model of a Multistage Bladed Rotor With Geometric Mistuning via Modal Analyses of Finite Element Sectors," *ASME J Turbomach*, Vol. 134, No. 4, 2012, pp. 041001.

[17] Ganine, V., Legrand, M., Michalska, H., and Pierre, C., "A sparse preconditioned iterative method for vibration analysis of geometrically mistuned bladed disks," *Computers and Structures*, Vol. 87, No. 5-6, 2009, pp. 342 – 354.

[18] Mbaye, M., Soize, C., and Ousty, J.-P., "A reduced-order model of detuned cyclic dynamical systems with geometric modifications using a basis of cyclic modes," *ASME J Gas Turb Pwr*, Vol. 132, No. 11, 2010/11/, pp. 112502 (9 pp.).

[19] Craig, R. R. and Bampton, M. C. C., "Coupling of substructures for dynamic analysis," *AIAA Journal*, Vol. 6, No. 7, 1968, pp. 1313–1319.

[20] Beck, J. A., Slater, J. C., Brown, J. M., and Cross, C. J., "Component Mode Reduced Order Models for Geometric Mistuning of Integrally Bladed Rotors," *AIAA Journal*, Vol. 52, No. 7, 2014, pp. 1345–1356.

[21] Fortescue, C. L., "Method of Symmetrical Co-Ordinates Applied to the Solution of Polyphase Networks," *Transactions of the American Institute of Electrical Engineers*, Vol. XXXVII, No. 2, july 1918, pp. 1027 –1140.

[22] Garzon, V. E. and Darmofal, D. L., "Impact of Geometric Variability on Axial Compressor Performance," *ASME J Turbomach*, Vol. 125, No. 4, 2003, pp. 692–703.

[23] Brown, J. M. and Grandhi, R. V., "Reduced-order model development for airfoil forced response," *International Journal of Rotating Machinery*, Vol. 2008, 2008, pp. 12 Pages.

[24] Sinha, A., Hall, B., Cassenti, B., and Hilbert, G., "Vibratory Parameters of Blades From Coordinate Measurement Machine Data," *ASME J Turbomach*, Vol. 130, No. 1, 2008, pp. 011013.